Scientific service framework for Copernicus sea and sea-ice surface temperature product improvement and CAL/VAL tool development and evolution

Activity 1: Improvement to Sentinel-3 SLSTR sea and sea-ice Surface Temperature product quality (WP A1-4)

[D2-A1_4] Technical report comparing SLSTR with other sensors

	Function	Name	Signature	Date
Prepared by	Project manager/ Project Team	Caroline RIBERE / Stéphane SAUX-PICART Anthony KETTLE		09/07/25
Approved by	Deputy CEO	Mahmoud EL HAJJ		09/07/25

Funded by the European Union's Copernicus programme

Document status

Scientific service framework for Copernicus sea and sea-ice surface temperature product improvement and CAL/VAL tool development and evolution Activity 1: Improvement to Sentinel-3 SLSTR sea and sea-ice Surface Temperature product quality (WP A1-4) [D2-A1_4] Draft journal article comparing SLSTR with other sensors-2024			
Issue	**Revision**	**Date**	**Reason for the revision**
1	0	17/03/2025	Initial version
1	1	05/06/2025	Incorporating the feedback from EUMETSAT
1	2	09/07/2025	Answering comments and making edits based on EUMETSAT feedback

Modification status				
Issue	Rev	Status *	Modified sections	Reason for the modification
1	1	M	All	Added references, and accepted reformulation suggestions from EUMETSAT
1	2	M	All	Answered comments from EUMETSAT and implemented suggested changes

* *I = Inserted* *D = Deleted* *M = Modified*

Funded by the European Union's Copernicus programme

Acronyms

AVHRR	Advanced Very High-Resolution Radiometer
BATS	Bermuda Atlantic Time-series Study station
ECV	Essential Climate Variable
EUMETSAT	EUropean organisation for the exploitation of METeorological SATellites
GHRSST	Group for High Resolution Sea Surface Temperature
IST	sea Ice Surface Temperature
METIS	Monitoring & Evaluation of Thematic Information from Space
MetOp	Meteorological Operational
MSG	Meteosat Second Generation
NOAA	National Oceanic and Atmospheric Administration
NWP	Numerical Weather Prediction
OSI SAF	Ocean and Sea Ice Satellite Application Facility
PO	Project Office
QL	Quality Level
Sci4MaST	Science for Marine Surface Temperature
SEVIRI	Spinning Enhanced Visible and Infra-Red Imager
SLSTR	Sea and Land Surface Temperature Radiometer
SST	Sea Surface Temperature
WP	Work Package

Funded by the European Union's Copernicus programme

Table of contents

Funded by the European Union's Copernicus programme

1. Introduction

1.1. Background

Sea Surface Temperature (SST) and sea-Ice Surface Temperature (IST) are key Essential Climate Variables (ECV) to understand the climate evolution and essential inputs to Numerical Weather Prediction (NWP) systems. Space observations represent a major asset since they provide global coverage, with often better than daily revisit frequency.

The European Organisation for the Exploitation of Meteorological Satellites (EUMETSAT) has major undertakings to contribute to a continuous delivery of high-quality surface temperature data over the Ocean and Sea-Ice. In particular, in the frame of Copernicus, EUMETSAT is in charge of the distribution of Sentinel-3 marine products, including SST and sea-IST derived from the Sea and Land Surface Temperature Radiometer (SLSTR). EUMETSAT is also in charge of technically managing the Group for High Resolution Sea Surface Temperature (GHRSST) Project Office (GHRSST-PO) on behalf of Copernicus.

The Science for Marine Surface Temperature (Sci4MaST) service is tasked with improving Sentinel-3 Sea and Land Surface Temperature Radiometer (SLSTR) Sea and sea-ice Surface Temperature (SST/IST) product quality. This report focuses on the consistency across all of EUMESAT's SST products and steps towards their harmonization.

1.2. Scope

This document is deliverable [D2-A1_4] Draft journal article comparing SLSTR with other sensors. It presents an overview of the journal article that will be published to summarise the findings relative to this study.

1.3. Content

In addition to this introductory chapter, this document includes the following chapter:

- §2, presenting the full report draft, including references and appendix.

Funded by the European Union's Copernicus programme

2. Draft journal article

This section presents a draft of the journal article. It is formatted for the delivery, but will be adjusted to fit the guidelines of the journal chosen.

2.1. Title, author list and journal

The proposed article title for this publication is:

"Comparison of Operational Sea Surface Temperature from MetOp/AVHRR and Sentinel-3 SLSTR"

It has not yet been decided which journal the article will be published in. This will be discussed further in the project with all stakeholders.

The proposed authors list for this publication is:

A.J. Kettle[(1)], S. Saux Picart[(1)], C. Ribere[(2)], M. El Hajj[(2)], G. Corlett[(3)], I. Tomažić[(3)], A. O'Carroll[(3)]

[(1)] Météo-France, Lannion, France

[(2)] NOVELTIS, Labège, France

[(3)] EUMETSAT, Darmstadt, Germany

2.2. Publication plan

The proposed publication plan is as follows:

- Abstract
- Introduction
- Datasets
- Methodology
- Intercomparison results
- Conclusion
- References

This publication plan will be updated if needed, based on the chosen target journal's requirements and once the draft has been finalized.

2.3. Abstract

This study presents the results of a sea surface temperature (SST) comparison analysis between the satellite sensors MetOp-B AVHRR and Sentinel-3 SLSTR over a three-month period from January to March 2023. Working with source data sets from each satellite, an intercomparison SST product was generated, identifying overlaps between the granules of the two satellites within a time interval of plus or minus 1 hour, and projecting Sentinel-3 SLSTR pixels onto the MetOp-B granule grid. Each granule of the intercomparison product had paired temperature retrievals for a number of overlapping pixels that could extend up to almost a million points. Summary statistics of the temperature differences of the matching pairs were calculated for each granule as well as information on the wind speed and solar zenith angle. The night-time Sentinel-3a SLSTR sea surface temperature was cooler by about 0.2 K compared to the MetOp-B AVHRR data, which was an expected feature arising from the applied SST algorithms for these satellite sensors. An unexpected finding from the analysis is a mismatch in the spatial temperature features between the two satellites along certain frontal areas. An analysis of SEVIRI geostationary temperature data ruled out rapid atmospheric features as the cause, and the origin remains unexplained.

Funded by the European Union's Copernicus programme

2.4. Article content

2.4.1. Introduction

The merging of satellite sea surface temperature fields requires their alignment to a common reference standard so that measurements can be combined across various sensors throughout the historical archive of measurements extending to the early 1980s. Because the measured temperature varies significantly in the near surface of the ocean on sub-diurnal time scales, any harmonization activity must also take this into account when comparing measurements among different satellite sensors. An additional complication is introduced by infrared sensors and microwave radiometers having differing characteristic depth scales of detection of near surface temperatures (Gentemann et al., 2009). While near surface temperature measurements from early satellite retrievals may be used to assess first order ocean mixing processes without sophisticated calibration procedures (Stramma et al, 1986), the quantification of near surface temperature for climate applications requires a harmonization procedure to ensure bias avoidance in measurements from successive satellite platforms at the 0.1 K level. Merchant et al (2019) conducted a comprehensive cross platform harmonization procedure of satellite-retrieved sea surface temperature products, extending to the early 1980s. Harmonization of different SST products was noted as one the target requirements of the community in the summary paper of O'Carroll et al. (2019).

The aim of this work is to understand differences between SST products from the MetOp/AVHRR and Sentinel-3/SLSTR platforms. Because of the different ways that the two satellite pairs are derived it was already known that the two SST products would have differences when generating statistics from large numbers of matching pixel information. The objective of this work was to understand the magnitude of the offset difference, its spatial distribution, and possible links with ancillary geophysical information like wind speed.

2.4.2. Datasets

The MetOp program comprises a group of three low-Earth orbit satellites, the first of which (MetOp-A) operated from 19 October 2006 to November 2021. Currently, there are two MetOp satellites in operation: MetOp-B, launched in 17 September 2012, and MetOp-C, launched in 7 November 2018. The satellites are in a sun-synchronous orbit with an inclination of 98.7 degrees to the equator and a mean altitude 817 km. The orbital period is 101.0 minutes and the satellites cross the equator on the ascending node at 21:30 local time. The orbit has a 29 day repeat cycle. MetOp-B and MetOp-C are phased approximately 180 degrees apart, and surface features seen by one satellite are overflown by the other satellite approximately 50 minutes later (Wikipedia-MetOp, 2025). The MetOp satellites carry the Advanced Very High-Resolution Radiometer (AVHRR), an instrument that has been used on U.S. satellites from 1978, including the NOAA series from 1979. The first instrument was a 4-channel radiometer, and the AVHRR/3 version on the MetOp satellites is a 6-channel instrument that was first carried on NOAA-15, launched in May 1998. The swath width of the instrument is approximately 2500 km, and the pixel resolution is 1.1 km at the nadir (EUMETSAT MetOp, 2025; EUMETSAT OSISAF, 2025; Wikipedia-AVHRR, 2025). The procedure for the derivation of AVHRR SST for MetOp-B and MetOp-C data is described in EUMETSAT OSISAF (2025). Marsouin et al. (2015) presents the background for the processing of the AVHRR data on MetOp-A outlining how quality level is assigned, and how regional/seasonal biases in SST retrievals are overcome using atmospheric profiles from numerical weather prediction models.

The Sentinel-3 satellite program comprises a group of two satellites: Sentinel-3A, launched on 16 February 2016 and Sentinel-3B, launched on 25 April 2018. The satellites have a sun-synchronous orbit with an inclination of 98.65 degrees and a mean altitude of 814.5 km. The orbital cycle is approximately 100.99 minutes with the local time of the descending mode at 10:00 local time. The orbit has a 27 day repeat cycle (385 orbits per cycle). The two satellites have the same orbit but are 140 degrees out of phase. As for the MetOp satellite pair, surface areas that are overflown by one satellite will be overflown by the other satellite some 10's of minutes later (Coppo et al, 2010, Wikipedia-Sentinel3, 2025; Copernicus-s3-mission, 2025). The Sentinel-3 satellites carry the SLSTR instrument, which is an 11-channel radiometer with a combination of visible and thermal infrared channels. The instrument was designed to retrieve land and surface temperatures, as well as fire radiative power, and two of the wavelength channels are devoted to this application (Bonekamp et al, 2016). Ground pixel radiances are retrieved through a system of scans by two rotating mirrors with different angles to the axis of rotation and covering different swathes at the surface (Sentinels-user-guides, 2025). This

Funded by the European Union's Copernicus programme

allows a view of sea surface through several viewing angles through the perturbing influence of the atmosphere. Each of the mirror rotations takes in views of the ground surface as well as calibration units for the infrared and visible channels. The instrument calibration relies on internal reference, with in situ measurements used as validation checks. The procedure for SST retrieval is described in Embury et al. (2012).

Table 1 - Information on satellite orbit and SST instrument for MetOp-B/AVHRR and Sentinel-3A/SLSTR

Satellite	MetOp-B[a]	Sentinel-3A[b]
Altitude	817 km	814.5 km
Inclination	98.7 degree	98.65 degree
Period	101.0 minutes	100.99 minutes
Cycle	29 days	27 days
Equator crossing time	21:30 ascending	10:00 descending
Instrument	**AVHRR[c]**	**SLSTR[d]**
Spectral channels	Channel 1: 0.58-0.68 µm Channel 2: 0.725-1.00 µm Channel 3A(6): 1.58-1.64 µm Channel 3B: 3.55-3.93 µm Channel 4: 10.3-11.3 µm Channel 5: 11.5-12.5 µm	Thermal IR: 3.7, 10.8, 12 µm Fire channels: 3.7, 10.8 µm Short wave: 0.55, 0.67, 0.87, 1.375, 1.6, 2.25 µm
Pixel resolution	1.1 km	1 km
Swath width	~2500 km	~740 km, ~1400 km
Product	**OSISAF[e]**	**EUMETSAT[f]**
Quality level description	0: unprocessed 1: cloudy 2: bad 3: suspect 4 acceptable 5 excellent	0: no data; land 1: bad data; T_{11} < 260 K, SST < 271.15 K, ice detected, NWP missing 2: worst quality; θ_{sat} > 55 3: low quality; twilight (87.5° < θ_{sat} < 92.5°) 4: acceptable quality; aerosol detected; abs(ASDI) > 0.2 (dual view only) 5: best quality

Notes:

[a] EUMETSAT OSISAF (2025), Wikipedia-MetOp (2025)

[b] Wikipedia-Sentinel3, 2025; Copernicus-s3-mission, 2025

[c] EUMETSAT OSISAF (2025)

[d] Sentinels-user-guides (2025)

[e] EUMETSAT OSISAF (2025),

[f] Corlett (2025), EUMETSAT-Sentinel3 (2025)

Funded by the European Union's Copernicus programme

2.4.3. Methodology

2.4.3.1. Building the Analysis Dataset

Granule files for MetOp-B/AVHRR SST (AVHRR-B) were available at MeteoFrance.Three months (January to March, 2023) of Sentinel-3A/B SLSTR granule data were made available from EUMETSAT by ftp transfer, of which only the data for Sentinel-3A SLSTR (SLSTR-A) were used in the AVHRR-B comparison in this report. The data for both sets of satellites were packed in NetCDF files with a number of ancillary parameters, including quality flags, a model wind speed product, and day/night information or solar zenith angle, among others. The information contained in NetCDF files for each satellite was different with much more information in the AVHRR-B files, including solar zenith angle and wind direction from the numerical weather product.

The analysis was carried out through several steps:

1. Census of AVHRR-B granules to obtain their overflight times and corner coordinates
2. Census of Sentinel-3 granules to obtain their overflight times and corner coordinates
3. Cross-comparison of the AVHRR-B and Sentinel-3A granule results assess to possible matches based on spatial overlaps and closeness-in-time
4. A production step wherein the cross-comparison results were used to read in and compare matching AVHRR-B and Sentinel-3A granules, and produce a set of composite NetCDF files.

The census of the AVHRR-B granules was carried out with the program structure shown in Appendix A to generate a summary ASCII file of the granule time and spatial information. The program was configured to run through one month of granules per run, with each month taking about 10 h to complete. For the project intercomparison objective, months January, February, and March were run to generate files ‘output01_jan.txt’, ‘output02_feb.txt’, and ‘output03_mar.txt’ in the directory Data_middle/Archive/.

The census of Sentinel-3 granules was carried out with the program structure shown in Appendix B to generate a summary ASCII file of the granule time and spatial information. The program was configured to run through all the granules for one Sentinel-3 satellite for the 3 months of available data (i.e., about 40000 granules). A single processing run would take about 39 h for one satellite. The processing of the Sentinel3A satellite was interrupted part way through its processing cycle, and its output is contained in two files: s3a_output20240422_p1.txt and s3a_output202424_p2.txt in the directory Data_middle/Archive. The processing cycle of Sentinel3B was uninterrupted, and its output is contained in the file s3b_output20240426.txt in the same directory. In processing granules, it was noted that there were sometimes irregularities in the ‘dtime’ field (i.e., the measurement time offset in seconds of the pixel with respect to the granule time stamp), which sometimes had values > 300 s. The origin of the problem is unknown, and the counts of these irregular pixels were output in the final column of the census files.

The subsequent step used the AVHRR-B and Sentinel-3A census information to assess possible overlap matches between the individual granules of each data set (Appendix C). This program took about 10 minutes to run and the step was necessary because the re-projection and production step (below) was computationally expensive. A match in time was identified if the Sentinel-3A granule time stamp occurred ±1 h of AVHRR-B time stamp, and this is consistent with previous intercomparison studies (Embury et al., 2012). A possible match of the granule areas was identified if there was an overlap of the latitude and longitude ranges. The time range considered meant that each AVHRR-B granule was typically associated with 2-6 Sentinel-3A granules with 3 being the most common value. However, because the granules of both satellites were oriented obliquely, AVHRR-B and Sentinel-3A granules that passed the initial spatial test may not have had any overlap, and the overlap issue was resolved in the following production step.

In the production step, composite NetCDF files with AVHRR-B and Sentinel-3A information were generated (Appendix D). First, AVHRR-B granule information was read in followed by the information from each matching Sentinel-3A granule in sequence. The Sentinel-3A data was reprojected on the AVHRR-B grid with the kd_tree.resample_nearest function of pyresample with the following flags set: radius_of_influence=2000.0 and epsilon=0.5. The Sentinel reprojection may have resulted in no coincident high-quality pixels from each satellite, for example, if there was extensive cloud cover obscuring the surface or if the two satellite granules were oriented so as not to overlap at all. If the granules did overlap resulting in more than one coincident high-quality pixel (i.e., AVHRR-B quality level 3-5 and Sentinel quality level 5), the

Funded by the European Union’s Copernicus programme

following steps were conducted. Summary statistics of ancillary information were calculated for the collection of pixels showing high quality AVHRR-B and Sentinel SST data, and these were appended to an ASCII file of summary statistics. Then, a NetCDF file was written with the combined AVHRR-B/Sentinel information: AVHRR-B latitude and longitude, AVHRR-B SST, AVHRR-B quality level, AVHRR-B solar zenith angle, AVHRR-B wind speed, AVHRR-B aerosol optical depth, AVHRR-B aerosol optical depth, AVHRR-B satellite zenith angle, Sentinel SST, Sentinel quality level, Sentinel l2p flags, Sentinel algorithm type, Sentinel satellite zenith angle. Each output NetCDF granule had a size of approximately 115 MB. For the approximately 43000 AVHRR-B granules, this program was run in two steps to handle approximately half of the collection, with each step taking about 20 days to complete.

2.4.3.2. Coarse Analysis Methods

The product of this analysis was a set of over 62000 NetCDF files, each with information for a AVHRR-B granule (SST and ancillary parameters) and a nearby Sentinel granule (also SST and some ancillary information) that had been re-projected onto the AVHRR-B grid. For each NetCDF file, there could be up to several hundred thousand pixels with ancillary information so that the volume of data was large. The number of valid match-up pixels in each granule depended on how the AVHRR-B and Sentinel granules overlapped, cloud cover, as well as threshold chosen for the quality level.

Because of this data volume, a decision was taken at the start of the coarse analysis procedure to compare the two satellite SST products based on the statistics generated at the granule level. The SST retrievals from individual pixels had significant noise levels in each satellite product that tended to be averaged out in statistics. This approach emphasized value of granules that had the largest number of matchup pixels. A second consideration was the spatial and temporal placement of the granules. Embury et al (2012) had pointed that there were regional and seasonal biases in SST retrievals in earlier SST intercomparison studies that were linked with total column water vapour.

The initial analysis focussed on the metadata in ASCII summary table that was generated at the same time as the match-up granules. The aim was to understand the valid match-up pixel content of the granule collection as well as spatial location of the granules with highest number of matchup pixels. A histogram was used to understand the match-up pixel content of the granule collection, and the granules were assigned a quartile, decile, percentile, and per mille rank according to their match-up pixel content. Spatial plots (imagettes) of the granules with the highest number of match-up pixels were created, showing difference fields of Sentinel minus AVHRR-B SST fields as well as ancillary information for quality levels and Sentinel calibration algorithm. These were qualitatively assessed to understand possible links among SST differences and quality level, spatial distribution of the quality level flag, and possible artefacts in the SST retrieval procedure linked to the Sentinel calibration algorithm.

Biases arose from concentrating on the granules with the highest number of match-up pixels as they tended to be concentrated in cloud-free subtropical areas with the equator, mid-latitudes and high latitudes under-represented. Additionally, it was assessed that the retrieved SST comparison should be conducted using the highest quality level-5 products for each satellite. The metadata ASCII summary file was therefore re-analyzed to identify a collection of granules in each 10-degree latitude-longitude box across the global ocean areas, containing at least 1000 high quality matchup pixels. This resulted in up to ~110 granules being associated with each 10-degree latitude-longitude box.-Being given that the number of high-quality matchup pixels could span over 2 orders of magnitude with lower counts disproportionately represented, only the granule with highest number of matching pixels at quality level 5 was retained to represent the whole 10-degree latitude-longitude box. All the other granules were discarded. This was judged as the subset of the best quality match-up granules with global coverage. The procedure was conducted three times for the full granule collection, and for the night and day subsets separately, which are shown below.

2.4.3.3. Fine Scale Analysis Methods

The imagettes from the first part of the coarse scale analysis revealed certain biases in the retrieved SST between Sentinel and AVHRR-B. For example, certain imagettes showed a step change in SST difference corresponding to a boundary in the Sentinel field where two different calibration areas joined. An unexpected artefact was the presence of a fine-scale structure in the SST difference fields at certain locations, as if the Sentinel and AVHRR-B SST fields were somehow locally mismatched. It was uncertain if the artefact may have been due to a moving atmospheric feature that

Funded by the European Union's Copernicus programme

may have become apparent in the short time delay between the overpasses of the two satellites. To investigate the effect, a case study was conducted for one identified instance on 7 January 2023 using SEVIRI data from geostationary satellite product at Meteo-France.

2.4.4. Intercomparison results

2.4.4.1. Course Analysis

Central to the coarse analysis was to understand the number of match-up pixels in collection of granules from the production step, as this was important for deciding how to structure the analysis. This was achieved by the histogram in Figure 1, which shows that the number of matchup pixels varies across 5 orders of magnitude from 2 to > 800 000. The histogram is plotted on log-log axes, and this emphasizes that a large number of the granules had a small number of match-up pixels and would have limited value in generating stable statistics of sea surface temperature difference to compare the two satellite products. Figure 1 has the decile thresholds identified so that a decile-10 selection would include all granules with more than about 127000 matching pixels. The project focused on the granules with the higher number of matching points as delivering the most stable comparison statistics.

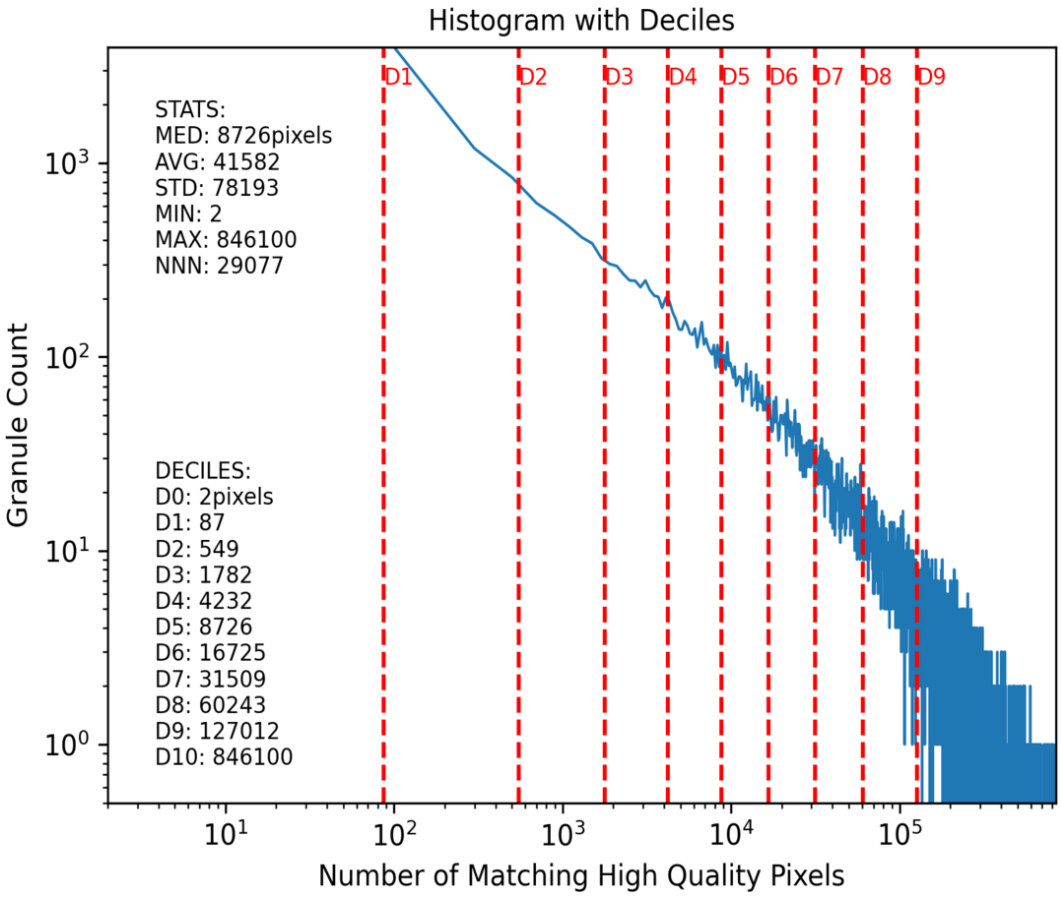

Figure 1 - Histogram of number matching granule pixels (for Metop quality level 3-5 and Sentinel-3A quality levels 5) on log-log axes with the decile divisions shown. This uses METOP granules 1-20000.

Funded by the European Union's Copernicus programme

The spatial distribution of the collection of granules across global ocean is shown in Figure 2. The points are colour-coded to show the approximate number of match-up pixels within the granule, with blue showing the location of half of the granule collection with less than about 8700 matching pixels, and red showing the decile-10 population, or 10% of the granule collection with the highest number of matching pixels. Qualitatively, the granules with the highest number of matching pixels tend to occur in cloud-free regions of the subtropics, and the trend becomes more pronounced when considering the highest percentile and highest per mille of the full granule collection. On the assumption that the granules with the largest number of overlapping pixels would generate the most stable statistics for assessing satellite SST differences, the 43 top-ranked granules (23 day and 20 night) were identified and statistics calculated for O(10^5) paired points of Sentinel-3A minus AVHRR-B SST difference. This yielded information that Sentinel-3A biased cold with respect to AVHRR-B at night-time with a median (standard deviation) SST difference of 0.19 (0.30) K, but biased warm during daytime with a median (standard deviation) SST difference of 0.01 (0.34) K.

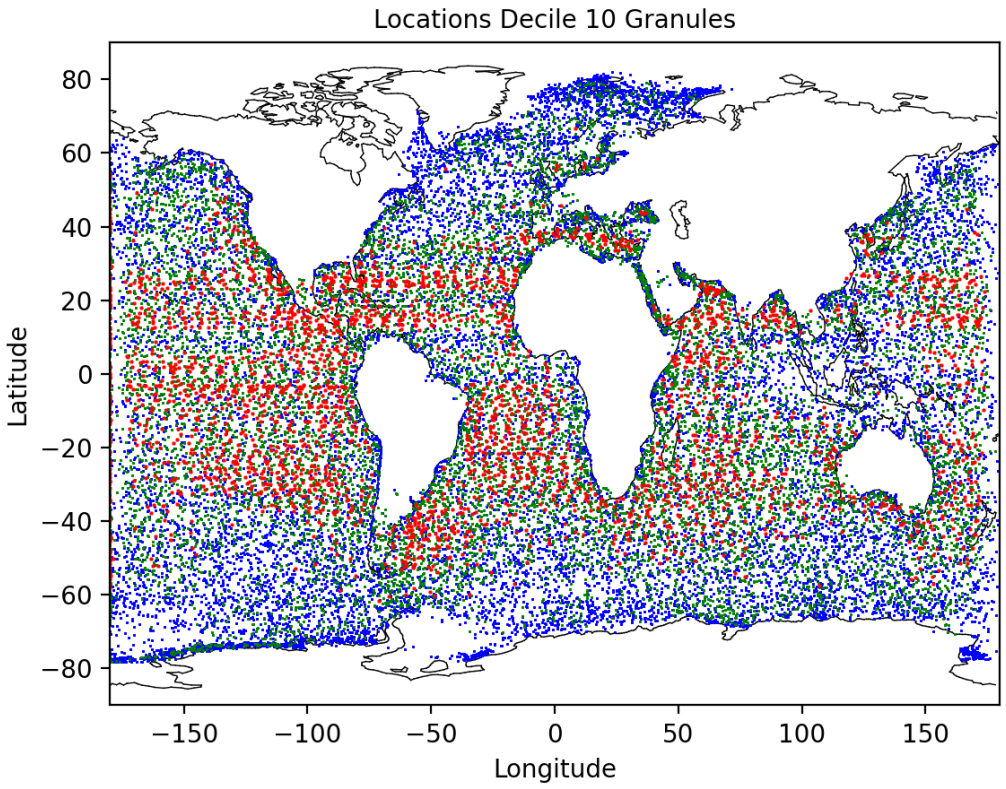

Figure 2 - Map of locations of the match-up granules with colour-coding for the relative number of pixels in the granule. Blue denotes the lowest number of match-up pixels per granule (decile1-5), green denotes an intermediate number of pixels (decile 6-9), and red denotes the highest number of pixels (evaluated at decile 10). Granules with the highest number of pixels generate the most stable statistics for the SST temperature difference between Sentinel-3 and MetOp, and these tend to be concentrated in cloud-free subtropical areas. This map was generated from MetOp granules 1-20000, or approximately half of the available dataset.

A global overview of the data set is achieved by considering the granule within each 10-degree latitude-longitude box with the largest number of matching pixels, and this is shown in Figure 3. Figure 3a and 3b show maps of the median of Sentinel-minus-AVHRR-B paired pixels for day and night, respectively. Figure 3c and 3d show maps of the standard deviation of this difference, also for day and night. The maps reveal large-scale patterns differences between low and high latitudes, and from the literature (Embury et al., 2012), this might be linked with total column water vapour.

Funded by the European Union's Copernicus programme

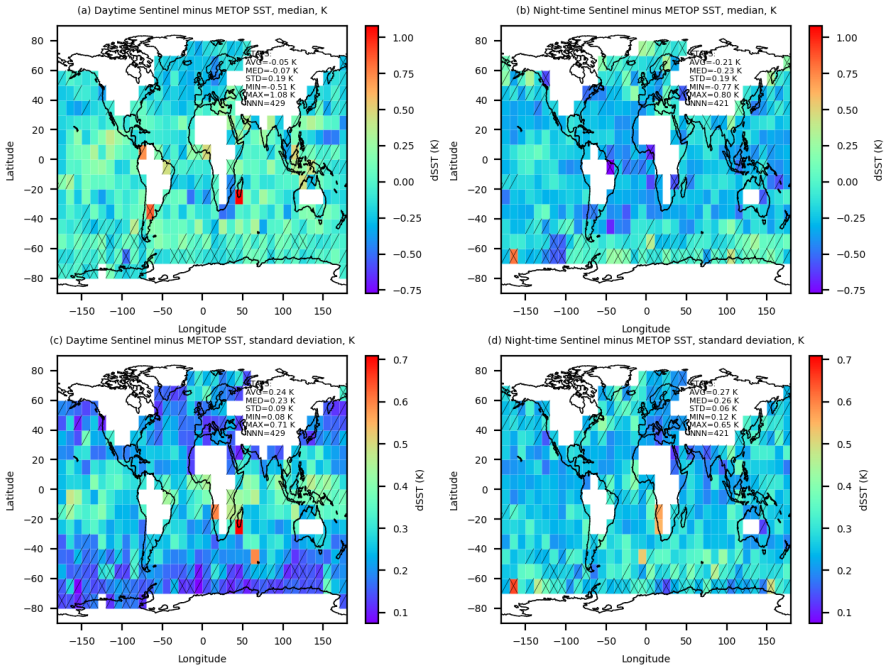

Figure 3 - Median of Sentinel-minus-AVHRR-B SST difference in 10 degree latitude-longitude squares for (a) daytime and (b) night-time, with standard deviations of the SST difference shown in (c) daytime and (d) night-time. Each 10 degree latitude-longitude box shows the results of the one granule (out of up to 120 granules) with the highest number of pixel matches at quality level 5 for both Sentinel-3 and AVHRR-B. Hatching has been applied to indicate the approximate number of matching pixels for the granule with a crossed-slash indicating 1000–10000 pixels, a single slash indicating 10000–100000 pixels, and no slash indicating >100000 pixels. A few identified granules in coastal or high with <1000 pixels have been removed from analysis because of unstable statistics.

2.4.4.2. Fine-Scale Analysis

As part of the coarse scale analysis, a series of detailed maps were created for the granules with the highest number of matching pixels to investigate the possible impact of quality level and calibration algorithm (Sentinel-3A) on possible biases on the SST difference fields. Figure 4 shows detailed information for one granule from the southern subtropical Atlantic Ocean near the coast of South America from 7 January 2023 at ~01:00 GMT.

Funded by the European Union's Copernicus programme

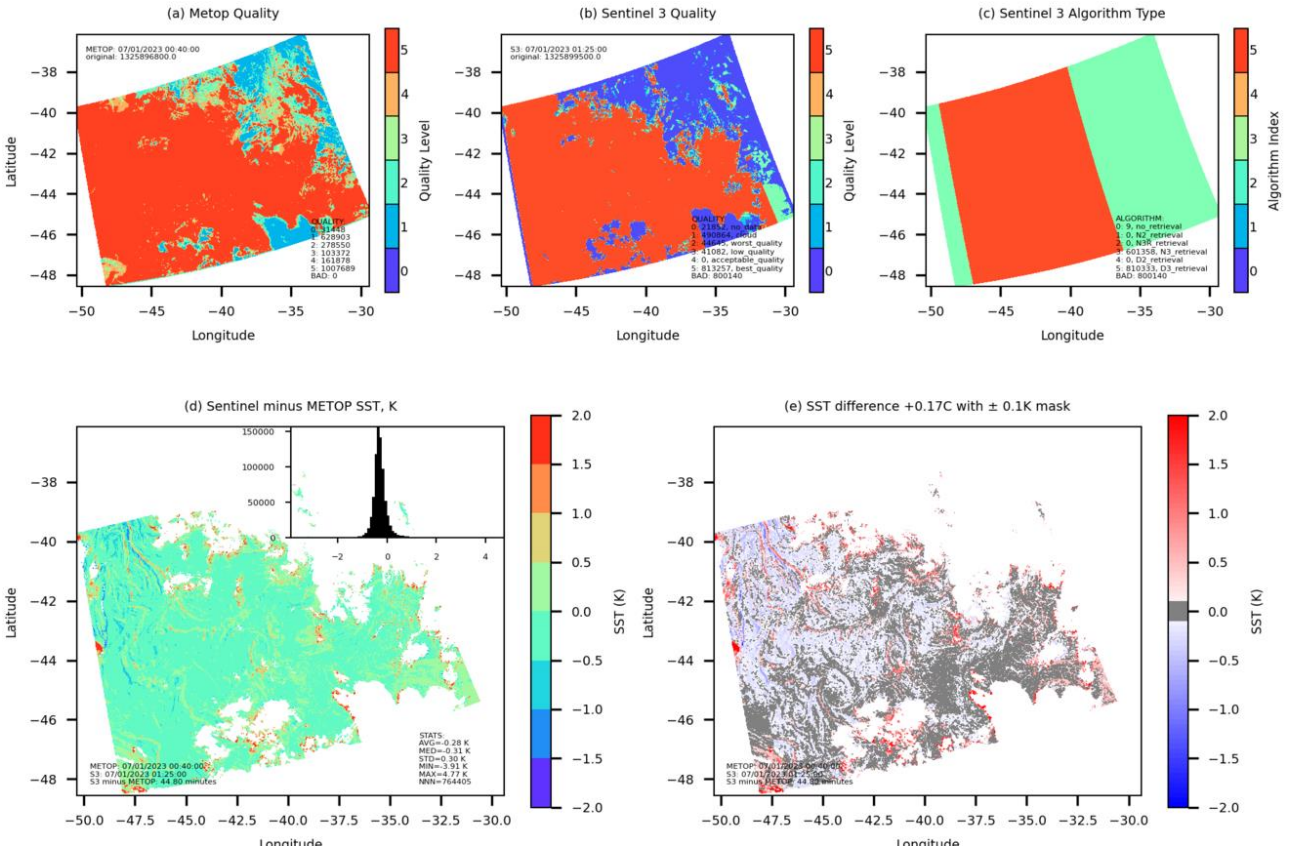

Figure 4 - Thumbnail plot with >640000 matching high quality pixels from netcdf file metop2885_s3a4. (a) AVHRR-B quality code, (b) Sentinel-3A quality code, (c) Sentinel-3A integer code for algorithm, (d) Sentinel minus METOP SST difference with inset histogram of pixel results, (e) same as (d) but with 0.17C added to field and a gray make applied in the range -0.1 to +0.1C.

From the information packed in the output NetCDF file, maps were plotted of the (a) AVHRR-B quality level integer, (b) Sentinel quality level integer, (c) Sentinel algorithm type integer, (d) Sentinel-minus-AVHRR-B temperature difference with an inset histogram showing how the Sentinel-3A data is biased cooler than AVHRR-B, and (e) Sentinel-minus-AVHRR-B temperature difference on a different colour scale. General observations of the results revealed that the largest differences between the two satellite products tended to occur in the vicinity of clouds. This observation contributed to the assessment that the comparison should be limited to the quality level 5 pixels of each satellite. Also, some plots of the SST difference field (but not Figure 4) showed SST discontinuities at the edges of the different SLSTR WST algorithm types.

Closer examination of top left part of the field in Figure 4d revealed localized banding features that could have resulted from a spatial mismatch between the AVHRR-B and Sentinel-3A granules. The feature occurs in relation to an atmospheric front. Because the two satellites captured images of the ocean surface with a time difference of some tens of minutes, there was a possibility that the banding pattern might have arisen from a travelling atmospheric feature that could have moved a significant distance between the overflight times of the two satellites. To investigate this, images from the Meteo-France geostationary satellite SEVIRI archive were analyzed across period of AVHRR-B/Sentinel overpass times. The geostationary satellite images have a time resolution of 15 minutes. Figure 5 shows a sample geostationary satellite image from 7 January 2023 at 00:00 GMT with a box outline showing the approximate location of AVHRR-B/Sentinel-3A overlap granule and banding feature in the bottom left-hand corner of the image. The figure highlights that AVHRR-B/Sentinel-3A comparison granule occurred near the edge of SEVIRI geostationary satellite product.

Funded by the European Union's Copernicus programme

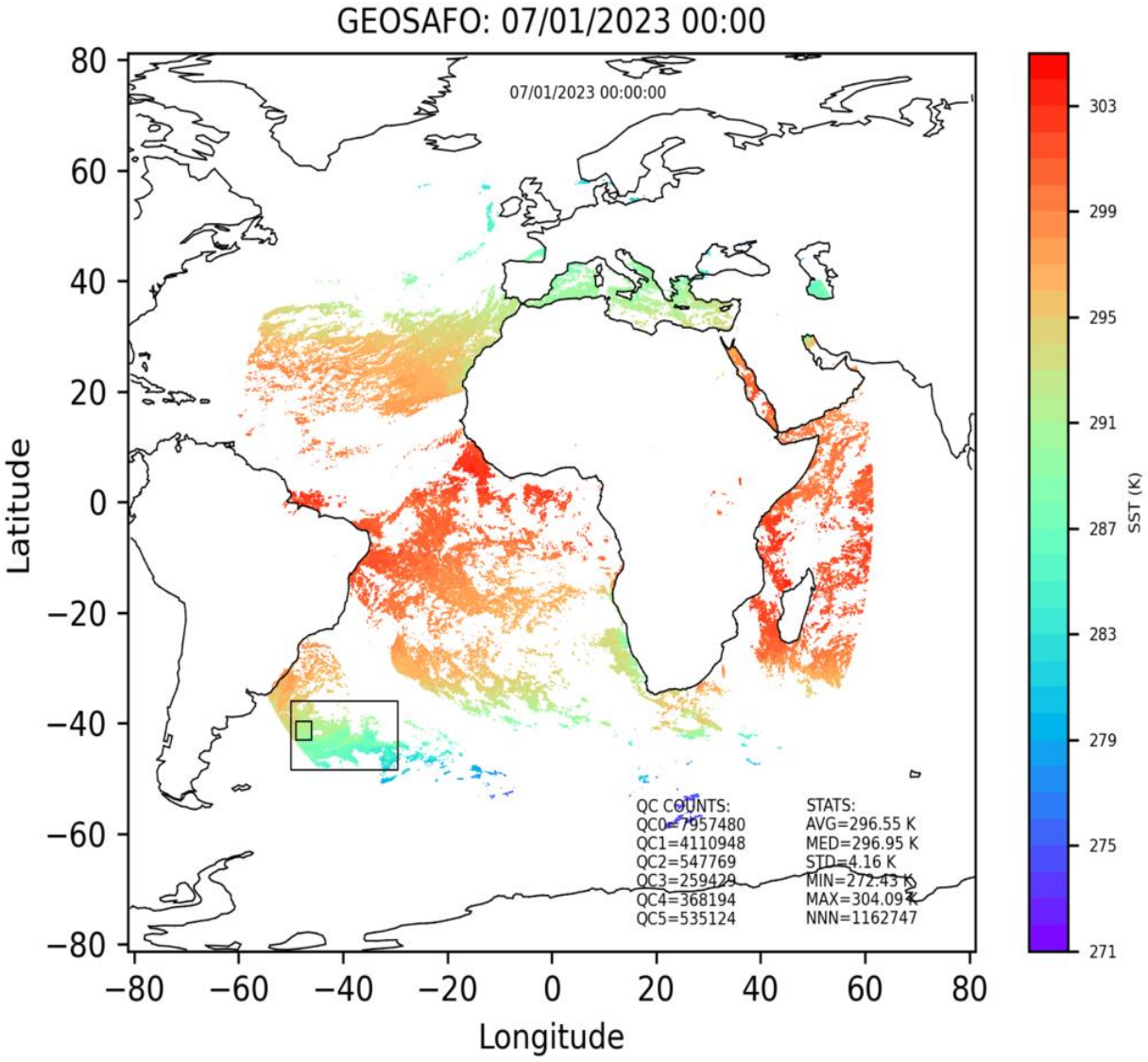

Figure 5 - Geostationary image of SST (quality levels 3-5) with the approximate location of the overlap granule from Figure 4 and the location of the banding feature in the bottom left part of the field.

The geostationary data was analyzed in a number of ways to understand the banding feature. First, a small segment of the geostationary satellite SST field was extracted and plotted in the same way as the AVHRR-B data (Figure 6). This showed that the two SST products were actually quite similar, both in terms of their spatial structure and in the values of SST. The geostationary satellite SST might have a lower spatial resolution, which would be expected from its greater distance. The second analysis was to calculate difference fields, subtracting successive geostationary satellite SST fields from a reference field established at 7 January 2023 00:00 (Figure 7). If the banding feature arose from a rapidly traveling atmospheric feature, then it would appear as a strengthening dipole in successful difference images. However, such a feature is not apparent in Figure 7, and the atmospheric cause for the banding can be discounted.

Funded by the European Union's Copernicus programme

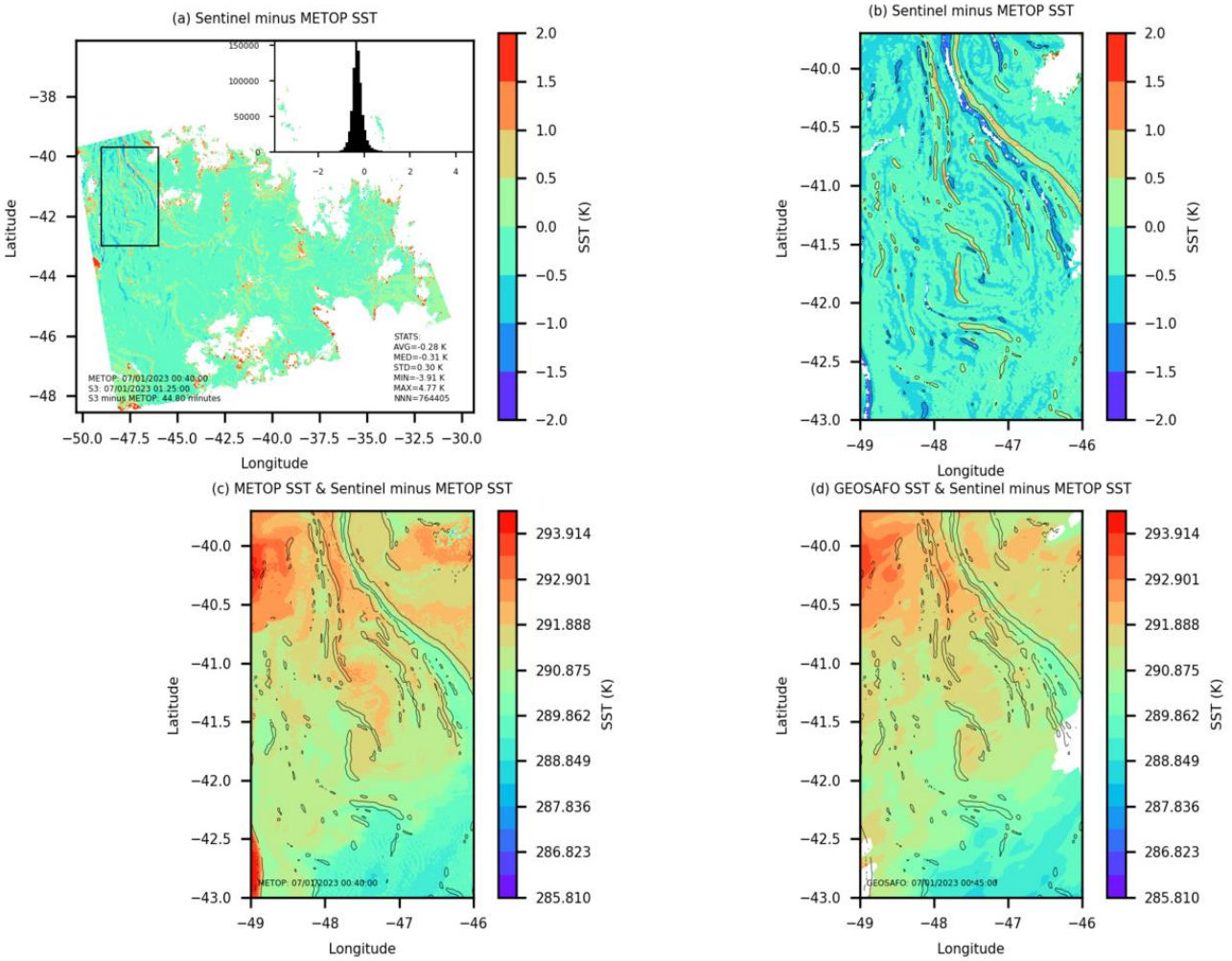

Figure 6 - (a) Sentinel minus AVHRR-B temperature difference from the SST granule information in netcdf file metop2885_s3a4 with a box surrounding the banding feature in left hand side of the plot, (b) close-up view of the banding feature in the temperature difference plot with contour lines overplotted, (c) AVHRR-B SST plotted in colour with the black contour lines reproduced from (b), (d) the geostationary satellite SST plotted in colour with the black contour lines reproducted from (b).

Funded by the European Union's Copernicus programme

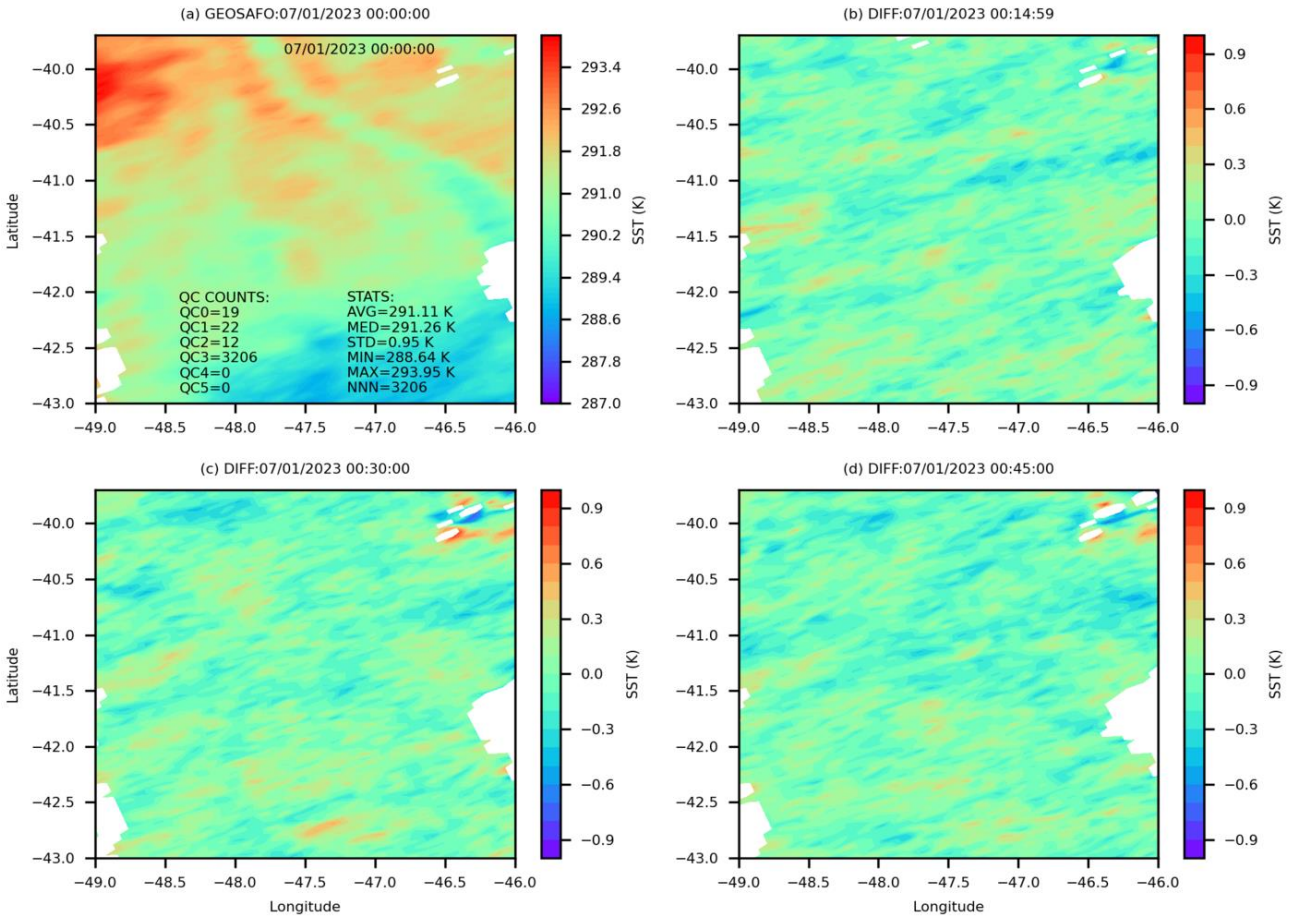

Figure 7 - (a) Geostationary satellite SST image for 7 January 2023 for the banding feature identified in AVHRR-B/Sentinel-3A comparison granule shown in Figure 4. Geostationary satellite SST difference fields with the (a) 00:15, (b) 00:30, and (c) 00:45 field subtracted from 00:00 field shown in (a).

2.4.5. Conclusion and discussion

A satellite intercomparison product was generated comparing AVHRR-B/AVHRR and Sentinel-3A/SLSTR over a three-month period from January to March 2023. Data from both satellites were packed in granules representing swaths of data over several minutes of satellite track. In the comparison product, overlapping granules between the two satellite products were identified, and the Sentinel-3/SLSTR pixel information was projected onto the AVHRR-B/AVHRR grid, giving a granule product with a number of overlapping points from which statistics were calculated. On the basis of median (standard deviation) statistics from a subset of the granules with the highest number of matching pixels Sentinel-3/SLSTR SST is cooler with respect to AVHRR-B/AVHRR by 0.19(0.30) K during night-time and warmer by 0.01(0.34) K during the day. The night-time differences likely arise from the cool-skin effect (Fairall et al, 1996) as the two satellite SST products are for different depths. During daytime, the nominal cool-skin effect is often obscured by solar heating of the upper ocean (Fairall et al., 1996) with the result that the temperature difference between the two satellites decreases or even reverses in low wind situations. The scatter in the comparison data, which is indicated by the standard deviation, is larger than the average cool-skin depression and also larger than the day-night differences on average. A case study of the temperature difference field from one granule match in western South Atlantic Ocean revealed a small-scale coherent structure linked to an ocean front. Analysis of SEVIRI geostationary SST data revealed that the feature was probably not an artefact of a moving atmospheric structure, but the origin of the feature remains unknown.

To model the near-surface heating effects for the purpose of correction or calibration of one satellite production with respect to the other, a simple model of the cool-skin/warm layer effect with an accuracy on the order of 0.02–0.1 K may be sufficient. The benefits of greater accuracy would not be apparent in the scatter of the satellite SST data. Current models for estimating near surface temperature gradients for satellite applications use upper ocean models (e.g., Price et al., 1986; Kantha and Clayson, 1994) with refined parameterizations for the absorption of solar energy (Gentemann et al., 2009) and the cool skin effect (Fairall et all, 1996).

2.4.6. References

Bonekamp, H., F. Montagner, V. Santacesaria, C.N. Loddo, S. Wannop, I. Tomazic, A. O'Carroll, E. Kwiatkowska, R. Scharroo, and H. Wilson: Core operational Sentinel-3 marine data product services as part of the Copernicus Space Component, Ocean Sci, 12, 787-795, 2016

Copernicus-s3-mission: https://sentiwiki.copernicus.eu/web/s3-mission, last access: 12 February 2025.

Coppo, P., B. Ricciarelli, F. Brandani, J. Delderfield, M Ferlet, C. Mutlow, G. Munro, T. Nightingale, D. Smith, S. Bianchi, P. Nicol, S. Kirschstein, T. Hennig, W. Engel, J. Frerick, and J. Nieke: SLSTR: a high accuracy dual scan temperature radiometer for sea and land surface monitoring from space, Journal of Modern Optics, 57, 1815-1830, 2010.

Corlett, G.: SLSTR SST Quality Level definitions – Day 2. document SLSTR_QualityLevels.pptx emailed 14 February 2025.

Embury O.,Merchant C.J., and Corlett G.K.: A reprocessing for climate of sea surface temperature from the along-track scanning radiometers: Initial validation, accounting for skin and diurnal variability effects, Remote Sensing of Environment, 116, 62-78, 2012.

EUMETSAT MetOp: Metop instruments, https://www.eumetsat.int/metop-instruments, last access: 25 Apr 2025

EUMETSAT OSISAF: Algorithms theoretical basis document for the low earth orbiter sea surface temperature processing (S. Saux Picart), GLB SST (OSI-201-b, OSI-201-c) NAR SST (OSI-202-c, OSI-202-d) MGR SST (OSI-204-b, OSI-204-c), version 1.9, 06/01/2025, Meteo France.

EUMETSAT-Sentinel3: Sentinel-3 sea surface temperature (SST) level 2 data guide, https://user.eumetsat.int/resources/user-guides/sentinel-3-sea-surface-temperature-sst-level-2-data-guide, 13 May 2024, last access; 20 February 2025.

Fairall, C.W., E.F. Bradley, J.S. Godfrey, G.A. Wick, J.B. Edson, and G.S. Young: Cool-skin and warm-layer effects on sea surface temperature, J. Geophys. Res., 101, 1295-1308, 1996.

Gentemann C.L., P.J. Minnett, and B. Ward: Profiles of ocean surface heating (POSH): A new model of upper ocean diurnal warming, J. Geophys. Res., 114, C07017, doi: 10.1029/2008JC004825, 2009.

Kantha, L.H., and C.A. Clayson: An improved model for geophysical applications, J. Geophys. Res., 99, 25235-25266, 1994

Marsouin, A., P. le Borgne, G. Legendre, S. Pere, and H. Roquet: Six years of OSI-SAF METOP-A AVHRR sea surface temperature data, Remote Sensing of Environment, 159, 288-306, 2015.

Merchant C.J., O. Embury, C.E. Bulgin, T. Block, G.K. Corlett, E. Fiedler, S.A. Good, J. Mittaz, N.A. Rayner, D. Berry, S. Eastwood, M. Taylor, Y. Tsushima, A. Waterfall, R. Wilson, and C. Donlon: Satellite-based time-series of sea-surface temperature since 1981 for climate applications, Nature Scientific Data, 6, 223, 2019.

O'Carroll, A.G., E.M. Armstrong, H.M. Beggs, M. Bouali, K.S. Casey, G.K. Corlett, P. Dash, C.J. Donlon, C.L. Gentemann, J.L. Hoyer, A. Ignatov, K. Kabobah, M. Kachi, Y. Kunhara, I. Karagali, E. Maturi, C.J. Merchant, S. Marullo, P.J. Minnett, M. Pennybacker, B. Ramakrishnan, R.A.A.J. Ramsankaran, R. Santoleri, W. Sunder, S. Saux Picart, J. Vazquez-Cuervo, and W. Wimmer: Observational needs of sea surface temperature, Frontiers in Marine Science, 6, 420, doi: 10.3389/fmars.2019.00420, 2019.

Funded by the European Union's Copernicus programme

Price, J.F., R.A. Weller, and R. Pinkel: Diurnal cycling: Observations and models of the upper ocean response to diurnal heating, cooling, and wind mixing, J. Geophys. Res. 91, 8411–8427, 1986.

Sentinels-user-guides: https://sentinels.copernicus.eu/web/sentinel/user-guides/sentinel-3-slstr/coverage, last access; 20 February 2025.

Stramma L., P. Cornillon, R.A. Weller, J.F. Price, and M.G. Briscoe: Large diurnal sea surface temperature variability: satellite and in situ measurements, Journal of Physical Oceanography, 16, 827-837, 1986

Wikipedia-AVHRR: Advanced very-high-resolution radiometer, https://en.wikipedia.org/wiki/Advanced_very-high-resolution_radiometer, last access: 12 February 2025.

Wikipedia-MetOp: MetOp, https://en.wikipedia.org/wiki/MetOp, last access: 12 February 2025.

Wikipedia-Sentinel3: https://en.wikipedia.org/wiki/Sentinel-3#cite_note-esa-eo-sent3-8, 12 February 2025.

Funded by the European Union's Copernicus programme